Sustained activation of P2X7 induces MMP-2-evoked cleavage and functional purinoceptor inhibition.

Christopher NJ Young[1], Natalia Chira[2], Justyna Róg[3], Rasha Al-Khalidi[2], Magalie Benard[4], Ludovic Galas[4], Philippe Chan[4], David Vaudry[4], Krzysztof Zabłocki[3], Dariusz C Górecki[2§]

From the [1]School of Allied Health Sciences, Faculty of Health and Life Sciences, De Montfort University, Leicester, LE1 5RR, UK, the [2]Molecular Medicine Laboratory, Institute of Biomedical and Biomolecular Sciences, School of Pharmacy and Biomedical Sciences, University of Portsmouth, PO1 2DT, UK, [3]Laboratory of Cellular Metabolism, Department of Biochemistry, Nencki Institute of Experimental Biology of the Polish Academy of Sciences, Pasteur Str., 02-093 Warsaw, Poland, the [4]PRIMACEN, Cell Imaging Platform of Normandy, Inserm, IBiSA and PISSARO Proteomic Platform, Institute for Research and Innovation in Biomedicine, University of Rouen; 76821 Mont-Saint-Aignan, France.

Running title: *MMP-2 cleavage as an off switch for P2X7 activity*

To whom correspondence should be addressed: [§]Dariusz C. Górecki, M.D., Ph.D., Professor of Molecular Medicine, Tel: +44 (023) 9284 3566 (office), +44 (023) 9284 3616 (lab); Fax: +44 (023) 9284 3565; E-mail: darek.gorecki@port.ac.uk

Keywords: P2X7, MMP-2, DMD, macrophage, β-dystroglycan, CD44, cancer

---

ABSTRACT

P2X7 purinoceptor promotes survival or cytotoxicity depending on extracellular ATP (eATP) stimulus intensity controlling its ion channel or P2X7-dependent large pore (LP) functions. Mechanisms governing this operational divergence and functional idiosyncrasy are ill-understood. We have discovered a feedback loop where sustained activation of P2X7 triggers release of active MMP-2, which halts ion channel and LP responses *via* the MMP-2-dependent receptor cleavage. This mechanism operates in cells as diverse as macrophages, dystrophic myoblasts, P2X7-transfected HEK293 and human tumor cells. Given that serum-born MMP-2 activity also blocked receptor functions, P2X7 responses *in vivo* may decrease in organs with permeable capillaries. Therefore, this mechanism represents an important fine-tuning of P2X7

functions, reliant on both cell-autonomous and extraneous factors. Indeed, it allowed evasion from the ATP-induced cytotoxicity in macrophages and human cancer cells with high P2X7 expression levels. Finally, we demonstrate that P2X7 ablation eliminated gelatinase activity in inflamed dystrophic muscles *in vivo*. Thus, P2X7 antagonists could be used as an alternative to highly toxic MMP inhibitors in treatments of inflammatory diseases and cancers.

INTRODUCTION

High concentration of eATP, which normally occurs in damaged tissues only, is one of the danger-associated molecular patterns (DAMPs). High (mM) eATP concentrations signal through the P2X7 purinergic receptor. Unlike other P2Xs, it is fully activated by significantly higher eATP and triggers the "danger" response in inflammatory cells (de Torre-Minguela et al., 2016). Therefore, P2X7 is a therapeutic target in inflammatory diseases (Bartlett et al., 2014). An interesting property of P2X7 is that this ATP-gated ion channel, under some conditions, can trigger non-specific passage of molecules of up to 900 Da. While the mechanism of this large pore (LP) opening is still disputed (Browne et al., 2013; Pippel et al., 2017), it is undoubtedly associated with cell death *via* a range of unique pathways (e.g. aponecrosis, autosis, etc.) and, as we recently discovered, with autophagy (Young et al., 2015). Further complexity of P2X7 response is illustrated by the findings that low-level eATP stimulation of this purinoceptor can result in tonic/trophic effects such as increased cellular glycolysis, proliferation, migration and invasion (Rigato et al., 2012; Amoroso et al., 2012; Xia et al., 2015). Studying purinergic abnormalities in Duchenne muscular dystrophy (Young et al., 2012; Sinadinos et al., 2015) we observed that myoblasts carrying a premature stop codon in the Dmd gene can display two markedly different modes of response to eATP: one extreme - autophagic cell death (Young et al., 2015) and the second, a cellular detachment response. Therefore, we have sought to elucidate the mechanism(s) governing this response diversity and allowing cells expressing high P2X7 levels to survive in the high eATP environment. We found the LP opening to be triggering the release of active matrix metalloproteinase 2 (MMP-2). Interestingly, while P2X7 activation was previously linked to MMP-9 release (Gu and Wiley, 2006) and MMP-2 and MMP-9 are both the gelatinases (Visse and Nagase, 2003; Page-McCaw et al., 2007), only the MMP-2 release is of functional consequences to the cell and the P2X7 receptor itself: We found P2X7-evoked MMP2 activity to regulate cell migration, invasion and remodeling of extracellular matrix and its receptors. We demonstrate, for the first time, P2X7-dependent cleavage of β-dystroglycan, a dystrophin-associated ECM receptor, in both myoblasts and macrophages. Importantly, we found that active MMP-2 released following LP formation also

cleaves P2X7 receptors. Therefore, we identified a novel feedback loop mechanism in which high eATP triggers P2X7 LP formation that regulates active MMP-2 release, which, in turn, halts the receptor function. Importantly, this mechanism afforded an evasion path from LP-induced cytotoxicity in cancer cells harboring high P2X7 levels.

RESULTS

Dystrophic myoblasts display increased MMP-2 activity, which is released upon P2X7 activation

The quantitative phosphoproteomic analysis of ATP-treated *mdx* myobalsts (from the *DMD*^{mdx} mouse model of Duchenne muscular dystrophy) revealed significant differences in the phosphorylation of the ERM proteins: Ezrin, Radixin and Moesin [Supplementary Figure S1A], with established roles in cell adhesion and migration (Yonemura et al., 1998; DesMarais et al., 2005; Li et al., 2007). Therefore, we performed cell migration and invasion assays and found that dystrophic cells treated with BzATP (300μM) became polarized in their direction of migration, whereas WT myoblasts moved more randomly [Supplementary Figure S1B]. Moreover, significantly increased migration and invasion rates through gelatin were observed for dystrophic myoblasts treated with 300μM BzATP [Supplementary Figure S1C, left panel]. These responses were completely blocked by the addition of the P2X7 antagonist A438079 or extracellular Ca^{2+} chelator EDTA [Supplementary Figure S1C, right panel] Given this invasion through gelatin, where MMPs have been implicated as downstream mediators (Xia et al., 2015; Qiu et al., 2014), we investigated the MMP activity in these cells.

P2X7-dependent MMP-9 release has been documented in peripheral blood mononuclear cells of mouse and human origin (Gu and Wiley, 2006). Surprisingly, in gel zymography (IGZ) (Vandooren et al., 2013) with gelatin immobilised in polyacrylamide gels revealed that dystrophic myoblasts display significantly elevated MMP-2 activity compared to WT myoblasts, while MMP-9 activity actually appeared reduced in dystrophic cell extracts (Figure 1A and Supplementary Figure S2). Where referred to throughout, 'MMP-2 activity' is used to indicate the presence of the enzymatically active mature form of MMP-2. Indeed, Western blotting analysis of these cell extracts revealed that MMP-2 protein levels were significantly lower in *mdx* than WT myoblasts (Figure 1B) thus excluding any possibility of a non-specific activation of MMP-2 during IGZ. Furthermore, MMP-9 protein expression was comparable across all samples (Figure 1B). Therefore, further investigations were focused on MMP-2. IGZ using cell pellets and supernatants collected from ATP stimulated *mdx* cells showed MMP-2 activity in cell pellets to fall over a period of 60 min following P2X7 activation, which correlated with the increased MMP-2 activity in supernatants (Figure 1C, D). Whilst MMP-9 did show a reduced signal in the pellet at 15 min, this was the same for both *mdx* and WT cells (the latter not expressing P2X7) and therefore not a P2X7-dependent response. BzATP (a more selective P2X7 agonist) evoked the same pattern of MMP-2 release and the concentration range triggering this effect was consistent with the P2X7 receptor activation (Supplementary Figure S3). Immunoblotting using anti-MMP-2 antibody confirmed the release of MMP-2 protein from cells (Figure 1E, F) into supernatants (Figure 1G, H). Elevated MMP-2 activity in supernatants was later followed by some LDH release indicating a degree of cell deaths (Figure 1H). Finally, MMP-2 activity changes were eliminated by the P2X7 large pore antagonist A438079 treatment (Figure 1I, J), further confirming this effect to be P2X7-specific.

MMP activity triggered by P2X7 pore formation leads to cleavage of β-dystroglycan and CD44

We next considered potential MMP-2 targets; given that β-dystroglycan in muscle is a well-known ECM receptor involved in cell adhesion and motility (Thompson et al., 2008) and that it has been shown to be a target for MMPs in different tissues (Yamada et al., 2001; Sbardella et al., 2015; Michaluk et al., 2007) we analyzed this protein by Western blotting. In dystrophic but not wild type myoblasts the P2X7 activation, shown previously to cause MMP-2 release, resulted in β-dystroglycan cleavage (Figure 2A, B). This effect was P2X7-dependent as it was absent in *mdx*/P2X7$^{-/-}$ cells (Xia et al., 2015) lacking P2X7 receptors (see Figure 4C). The resulting disruption of the link between the ECM and the cell membrane dystroglycan may explain the cell detachment response and enhanced migration of dystrophic cells (Supplementary Figure S1). CD44 is another known MMP target (Chetty et al., 2012), which is also an interacting partner of the ERM proteins (Visse and Nagase, 2003). Moreover, CD44 cleavage products have been shown to bind to and augment activation of P2X7 receptors (Moura et al., 2015). We therefore hypothesized that a similar mechanism may operate in dystrophic cells. Interestingly, while we found that CD44 cleavage did occur in *mdx* myoblasts (Figure 2C, D), it was not associated with the expected augmentation of P2X7 functions. In fact, we uncovered downregulation of P2X7 responses subsequent to MMP release.

MMP-2 is a suppressor of P2X7 receptor functions

In our previous work, we found P2X7-dependent pore formation and autophagic cell death to be completely absent in the presence of serum (>5%) in the medium (Young et al., 2015; Sinadinos et al., 2015). Given that the serum is a rich source of proteases including MMPs, cathepsins and trypsins (Thrailkill et al., 2005; Weitoft et al., 2015; Artigas et al., 1981), we investigated the possibility that the serum MMP-2 is a critical factor in mediating this P2X7 response inhibition. Indeed, P2X7-dependent MMP-2 release, measured by the decreasing activity in cell pellets, was only observed in serum-free media and completely blocked when myoblasts or macrophages were analyzed in high-serum (Figure 3A). P2X7 LP function measured by EtBr uptake was also inhibited by the increasing serum concentrations but only if the serum contained active MMP-2 (Figure 3B, C). Titration of MMP-2 inhibitor I (Millipore) showed that at 67μM it effectively blocked MMP-2 (Figure 3D) without affecting MMP-9 activity. Pre-incubation of cells with this compound resulted in significantly enhanced P2X7-evoked EtBr uptake (Figure 3E). Importantly, active MMP-2 (recombinant protein or present in a serum) inhibited specific P2X7 calcium channel activity too (Figure 3F). In contrast, inhibitors of cathepsins and trypsins, having, no effect on MMP-2 activity [Supplementary Figure S4A], were completely ineffective in altering P2X7 functions [Supplementary Figure S4B]. This confirmed the specific effect of MMP-2 on P2X7 (Figure 3G).

P2X7-dependent MMP-2 release occurs in macrophages and P2X7-transfected HEK293 cells

Next, we studied whether this mechanism is universal. Given the known P2X7 role in macrophages, we examined P2X7-dependent MMP-2 release in the RAW264 mouse macrophages (Figure 4A, B), in primary mouse peritoneal macrophages (Figure 4C, D) but also in HEK293 cells transfected with mouse P2X7 (HEK^{P2X7}, Figure 4H). Importantly, these HEK^{P2X7} showed no MMP-9 activity thus confirming the response to be MMP-2 specific. Macrophages displayed a more rapid release of MMP-2 in response to BzATP (Figure 4A), consistent with higher P2X7 receptor expression levels in these cells when compared to dystrophic myoblasts (Young et al., 2015). This response was again completely abolished in the presence of high serum (Figure 4A, B). Crucially, double negative primary macrophages isolated from *mdx*/$P2X7^{-/-}$ mice (Sinadinos et al., 2015) did not display intracellular MMP-2 activity or extracellular MMP-2 release in response to BzATP treatment, confirming the response to be P2X7 dependent (Figure 4C). Macrophages also displayed β-dystroglycan cleavage, which was completely absent in P2X7 knockout-derived cells (KO, Figure 4E). Indeed, this response was more rapid than in myoblasts; macrophages displayed complete cleavage of the 43 kDa β-dystroglycan band within 30 min of BzATP stimulation, which may again reflect the increased level of P2X7 expression in these cells. Interestingly, transfection of HEK cells with P2X7 [Supplementary Figure S5] was both necessary and sufficient to confer P2X7-dependent MMP-2 release from these cells in response to BzATP (Figure 4H).

P2X7 is a proteolytic target for MMP-2

Given the MMP-2 release in response to P2X7 activation and that this lead to down regulation of receptor functions, we investigated the possibility that P2X7 itself could be a target for MMP-2 cleavage. CleavPredict (Sandford Burnham) analysis revealed multiple putative cleavage sites for MMP-2 in mouse and human P2X7 sequences [Supplementary Figure S6A]. Therefore, we performed Western blotting with anti-P2X7 antibody in samples from BzATP-treated cells under conditions where MMP-2 is released. We found reduced levels of the 80 kDa P2X7 band 60 min after BzATP treatment (Figure 5A) and increasing amounts of a potential C-terminal cleavage product (~35 kDa) occurring after 30 min. This cleavage product was not present in samples pre-incubated with MMP-2 Inhibitor I (Figure 5A, lower panel). Significant cleavage was already observed 15 mins following P2X7 activation (Figure 5C). For a direct confirmation, protein lysates from *mdx* myoblasts, peritoneal macrophages and HEKP2X7 cells were incubated with activated or inactive recombinant mouse MMP-2 for 30 min at 37°C. We observed a cleavage product of the same molecular weight as that seen in BzATP-treated cells, when active recMMP-2 was used. This band was absent in samples treated with inactive recMMP-2 (Figure 5E). The size of this cleavage product (~35 kDa) corresponded with predicted cleavage sites at positions 277 and 298 (Figure 5G). The first site is particularly well conserved across species [Supplementary Figure S6B]. Combination of data obtained using recMMP-2 and its blocker in cells and in protein extracts confirmed that P2X7 is a trigger for the release as well as the proteolytic target for MMP-2.

MMP-2 release blocks P2X7 pore formation and ATP-induced death in tumor cells

P2X7 has been found up-regulated in tumors including as diverse types as breast (Ma, 2015), brain (Monif et al., 2014) and prostate (Qiu et al., 2014). Tumor cells were found to benefit from increased mitochondrial metabolic activity and growth caused by increased P2X7 expression (Di Virgilio et al., 2009). However, there is a question: How these cells avoid death associated with this high-level P2X7 expression and activation in high eATP environments? Discovery of the MMP-2-dependent P2X7 cleavage prompted us to investigate whether tumor cells exploit this mechanism to evade the cell death. Firstly, we interrogated the Cancer Genome Atlas database and found that over-expression of P2X7 and MMP-2 in prostate cancer samples coincide [Supplementary Figure S7]. We then confirmed very high levels of P2X7 receptor expression in the human LNCaP prostate cancer cells (Figure 6A). However, EtBr uptake in these cells following 30 min stimulation with 3mM ATP was not as strong as would be expected from such high P2X7 expression levels (Figure 6B) and there was no cell rounding, detachment or blebbing (data not shown). In contrast, a significant P2X7-dependent EtBr uptake was observed when MMP-2 activity was blocked (Figure 6B). In gel zymography showed constitutively high levels of MMP-2 being released from LNCaPs into the supernatant, which was further elevated in the presence of P2X7 agonists (Figure 6C). This high extracellular MMP-2 activity coincided with constitutively high levels of the P2X7 cleavage product (Figure 6A), which could explain these surprisingly low P2X7 responses in cancer cells despite a high-level receptor expression. Finally, the eATP-evoked cell death of LNCaPs in the LP-buffer was found very low and completely attenuated in the presence of MMP-2-containing serum but enhanced four-fold by the MMP-2 inhibitor (Figure 6D).

Therefore, this active MMP-2 release appears to be a universal protective mechanism, fine-tuning P2X7 receptor responses in various cell types, allowing stimulation sufficient for promoting growth and survival whilst minimizing pore formation and cell death.

P2X7 inhibition ablates gelatinase activity in mdx skeletal muscle in vivo

Upregulation of P2X7 receptor expression has been documented in a number of muscular dystrophies with an inflammatory component, including DMD and LGMD2b (Young et al., 2012; Sinadinos et al., 2015; Rawat et al., 2010; Gazzerro et al., 2015). Notably, we have recently demonstrated multifaceted beneficial effects of P2X7 ablation and pharmacological inhibition on DMD pathology (Sinadinos et al., 2015). Here we found that ablation of the P2X7 receptor in *mdx* mice also results in significant reductions in gelatinase activity in dystrophic skeletal muscles *in vivo*. Gelatinase activity in *mdx* muscles was found to be concentrated around populations of infiltrating inflammatory cells but, interestingly, also associated with nuclei of regenerating fibers (Figure 7A, upper right and inset panels). The significant reduction of this activity in muscles of *mdx*/P2X7$^{-/-}$ animals (Figure 7B) supports the finding of P2X7-dependent MMP-2 activity and highlights an important new pathological pathway that is ameliorated by P2X7 ablation (Sinadinos

et al., 2015). In contrast to this *in situ* activity, Western blotting showed no reduction in MMP-2 or MMP-9 protein levels in *mdx*/P2X7$^{-/-}$ compared to *mdx* muscles (Figure 7C). In fact, lower levels of MMP-2 were observed in *mdx* compared to WT lysates, indicating that dystrophic muscle retains the abnormal MMP-2 phenotype found in dystrophic myoblasts (Figure 1).

DISCUSSION

Enhanced migratory/invasive behavior following P2X7 activation led us to the identification of significantly elevated MMP-2 activity in dystrophic muscle cells, where P2X7 itself is upregulated. MMP-2 was released in a P2X7-dependent manner and effected the cleavage of β-dystroglycan and CD44 - well documented orchestrators of cellular attachment and migration. Surprisingly, MMP-2 release was found to coincide with the cessation of P2X7 functions. We demonstrated this to be due to the proteolysis of P2X7 by MMP-2. Based on these results, we propose that P2X7 signalling responses are modulated by a novel feedback loop involving MMP-2-evoked proteolytic processing, rendering the P2X7 non-functional. We demonstrated the universality of this mechanism by confirming it in macrophages and HEK293 cells expressing P2X7. We also demonstrated the clinical relevance of these findings by showing that P2X7 ablation abrogates gelatinase activity in dystrophic muscles *in situ*. Finally, we showed that MMP-2 inhibition triggers death of human cancer cells, which were otherwise unresponsive to eATP stimulation and thus the P2X7-dependent MMP-2 release represents a fine tuning mechanism for P2X7 receptor functions, imparting the ability to benefit from the P2X7 over-expression for growth and metabolism, whilst protecting against P2X7 large pore-induced cell death in the high eATP environment.

We propose that P2X7 possesses its own autocrine signalling feedback through MMP-2. We showed that MMP-2 cleavage does not differentiate between pore and channel activity, as both are blocked (Figure 3E & 3F). However, only during the high level or chronic stimulation, the LP becomes activated and MMP-2 is released, hence MMP-2 activity affects the pore over the Ca^{2+} channel function. This provides an elegant system of enzymatic tuning, which can regulate P2X7 signaling in every cell type. Cleavage predictions mapped the MMP-2 sites to residues R277 and 298 (Figure 5G). The first region is particularly well conserved across the species [Supplementary Figure S6B] and indeed we found this mechanism operant in human and mouse cells. Moreover, this region has been reported to harbour the P2X7 gain of function mutation, R276A (Thompson et al., 2010). We therefore hypothesise that this gain of function is conferred through the ablation of this MMP-2 site, as confirmed by CleavPredict and further experiments are underway to ascertain whether cleaved domains of P2X7 retain any function.

Overall, this work provides new insight into the molecular mechanisms of P2X7 function and regulation orchestrating the purinergic signalling (Figure 8). It is interesting to consider the

physiological implications of this mechanism, where P2X7 expressing cells would respond to high eATP differently: The same receptor density on the same cell may produce a significantly different effect in organs with discontinued capillaries (sinusoids) permitting serum proteins, including MMP-2, to leave the bloodstream. Therefore, sinusoids in the liver, endocrine, lymphoid and hematopoietic organs (e.g. spleen and bone marrow) present P2X7 with a working environment entirely different to that in the CNS, sheltered behind the blood-brain barrier. Moreover, in pathological conditions disrupting integrity of blood vessels or BBB functions, P2X7 functions may change significantly.

Moreover, P2X7 has established roles in cell migration and invasion, with notoriety in tumour metastasis, where MMPs have been implicated as downstream mediators of the eATP response (Xia et al., 2015; Qiu et al., 2014). We have shown inter-dependence of these responses and identified β-dystroglycan as a target. Dystroglycan is also a known component of focal adhesions in myoblasts (Kwan et al., 2004). Interestingly, we found P2X7-dependent MMP activity associated with central nuclei of regenerating myofibers, which raises questions about its function there; MMP-2 in cardiomyocyte nuclei might cleave PARP, a DNA-repair enzyme (Schwarz et al., 2012). However, although intracellular MMP-2 activity has been demonstrated, including in skeletal muscles (Hadler-Olsen et al., 2015), mechanisms governing the balance between intra- and extracellular MMP-2 remain elusive (Ali et al., 2012).

In both skeletal muscles and muscle cells, we found significantly elevated MMP-2 activity, yet MMP-2 protein levels were downregulated compared to WT. Clearly, expression of MMPs cannot be used as an indicator of its activity as the latter is controlled in a complex manner involving the tissue inhibitors of metalloproteinases (TIMPs). However, the release of MMP-2 correlated with shifting its activity from intra to extracellular compartments, suggesting that it was due to changes in MMP-2 localisation and not because of its associated TIMPs. P2X7 expression is upregulated in several human cancers (Adinolfi et al., 2012) and P2X7 has been implicated in tumor growth-promotion (Di Virgilio et al., 2009; Di Virgilio, 2015). Intriguingly, cancer cells appear to be able to reap the rewards of elevated P2X7 receptor expression without suffering the consequences of LP-associated cell death. The molecular mechanisms behind this remarkable paradox were a mystery. Here we show for the first time that cancer cells are able to benefit from the P2X7 tonic stimulation without succumbing to P2X7 toxicity through MMP-2 release causing direct receptor cleavage. cBioportal (Cerami et al., 2012) analysis of P2X7 and MMP-2 expressions in the Cancer Genome Atlas (TCGA) showed upregulation of both mRNAs in all tumor types [Supplementary Figure S7A] with a strong correlation between expression levels in prostate cancers [Supplementary Figure S7B]. Indeed, we have confirmed this P2X7 cleavage in the human LNCaP prostate cancer cells.

In therapeutic terms, we have shown reduced gelatinase activity in areas of infiltrating macrophages in *mdx*/P2X7$^{-/-}$ muscles at the height of the pathology in these animals. Therefore, P2X7 antagonism shown to inhibit fiber damage, myogenic cell death and reduce inflammation (Sinadinos et al., 2015), also involves MMP inhibition. MMP-9 ablation in *mdx* mice has documented beneficial effects, with reduced levels of necrosis and neutrophil invasion but only at the acute disease phase (Shiba et al., 2015; Hindi et al., 2013). Interestingly, MMP-2 ablation has been shown to impair both angiogenesis and myofiber regeneration in *mdx* model (Miyazaki et al., 2011). This data highlights the problem with global MMP inhibition. Our results suggest that P2X7 receptor antagonists may offer a targeted alternative to the global MMP antagonism, preventing the serious side effects associated with such treatments (Cathcart et al., 2015). Receptors are more "druggable" and several P2X7 antagonists are already available (Bartlett et al., 2014); this approach might be applicable to a host of MMP-associated pathologies, including infectious diseases (sepsis), cancer, rheumatoid arthritis, atherosclerosis, inflammation, cardiomyopathy and, last but not least, muscular dystrophies.

Given that both MMP-2 and MMP-9 gelatinases can be released following P2RX7 stimulation, it is remarkable that MMP-2 knockout exacerbated inflammatory arthritis while MMP-9 knockout reduced it (Itoh et al., 2002; Xue et al., 2014). Moreover, MMP-2 mutation causes a multicentric osteolysis and arthritis syndrome in humans (Martignetti et al., 2001). Our data provide molecular insight into this divergence as MMP-2 ablation would eliminate the natural "off" switch for pro-inflammatory P2X7.

In conclusion, our results provide a novel mechanistic insight into the molecular signalling pathways associated with the elusive P2X7 large pore; the MMP-2 feedback loop we described here represents a first indication of how physiological niches can regulate P2X7 pore function through variations in serum concentration or MMP-2 uptake/release. The implications of this are significant for both immunology and pathology, given the important roles of both P2X7 and metalloproteinases in inflammatory and degenerative disorders (Cauwe et al., 2010). Finally, we postulate that P2X7 functions *in vivo* can vary significantly between the same cell type located in organs with different serum accessibility e.g. spleen and brain. This mechanism may also explain why, in tumors, high density of P2X7 in the presence of high eATP does not lead to P2X7- driven cell death.

MATERIALS AND METHODS

Animals

C57BL10, *DMD*^{mdx} (*mdx)* and *mdx*/P2X7$^{-/-}$ (Sinadinos et al., 2015) 8 week old male mice were used in accordance with institutional Ethical Review Board and the Home Office (UK) Approvals. All mice were maintained under pathogen-free conditions and in a controlled environment (12hr

light/dark cycle, 19-23°C ambient temperature, 45-65% humidity). Mice were killed by CO_2 inhalation and cells and muscles dissected and used for protein extraction, or frozen in isopentane pre-chilled in liquid nitrogen for cryosectioning.

Antibodies and reagents

The following antibodies were used at 1:1000: anti-P2X7 (177003, Synaptic Systems), anti-MMP-2 (TP220, Amsbio), anti-MMP-9 (TP221 Amsbio), anti-actin (A2066, Sigma), anti-GAPDH (G9545, Sigma), anti-HCAM/CD44, (Santa Cruz, sc-18849). Anti-F4/80 (Abcam, ab6640) was used at 1:200 and anti- β-dystroglycan (DSHB, MANDAG2(7D11)) was used at 1:50 dilution. Other reagents used: P2X7 antagonist A438079 (10μM, Tocris Bioscience), MMP-2 inhibitor I (Millipore). All other chemicals were purchased from Sigma. Agonists were used at concentrations of 3mM (ATP) and 0.5 mM (BzATP), unless stated otherwise.

Cell culture

Wild-type and dystrophic myoblasts (with a premature stop codon in exon 23 of the Dmd gene) (Browne et al., 2013) were cultured as primary cells in KnockOut DMEM (Invitrogen) supplemented with 10% v/v KSR (Knockout Serum Replacement, Invitrogen), 5% v/v DHS (Donor Horse Serum, Sera Labs) and 2mM L-glutamine. Peritoneal macrophages isolated by lavage with 5ml ice cold PBS-containing 1% FBS (Sigma) were maintained in 10% v/v FBS and 2mM L-glutamine. Raw264.7 mouse macrophages (ATCC) were cultured as per peritoneal macrophages. LNCaP cells (ATCC; CRL-1740™) were maintained in 50:50 DMEM F12 HAMS, RPMI 1640, supplemented with 10% v/v FBS (Sigma) and 2mM L-glutamine. Following cell culture cells were washed to remove all traces of serum and analyzed in an appropriate serum-free assay buffer.

Zymography

For IGZ, all experiments were conducted in serum-free physiological saline buffer (145mM NaCl, 5mM KCl, 1mM $MgCl_2$ and 10mM Na-HEPES). Subsequently, cells were scraped in lysis buffer containing 50mM Tris base, 0.5% v/v Triton, pH 7.4. 30-40g proteins were resolved in 10% poly- acrylamide (29:1) gels containing 2mg/ml gelatin (Sigma). Gels were washed 3x 30min in 2.5% Triton-X solution, washed in water, then left in the incubation buffer (50mM Tris HCl, 0.15M NaCl, 10mM $CaCl_2$, pH 8) for 24-48h. Gels were stained with Coomassie Brilliant Blue G (0.05%), de-stained in 8% AcOH and 4% MetOH and im- aged using GelDoc EZ system (Biorad). The protein bands staining intensity was used as a loading control [Supplementary Figure S2] and densitometric analyses were performed using the integrated density measurement function of the ImageJ software (Schindelin et al., 2012). *Ex-vivo*, *in situ* zymography was performed on 10μm cryosections of TA muscles. Muscle sections adhered to glass slides were rehydrated in IGZ incubation buffer (as above), DQTM Gelatin (0.2mg/ml) was added and sections were left overnight at 37°C and images were captured using LSM710 confocal (Zeiss). Cleavage site prediction was performed using CleavPredict (Sandford Burnham).

Western Blotting

Proteins were extracted from adherent cells by scraping in 100 µl ice-cold extraction buffer containing 1 x LysisM (Roche, 04719956001), 1x cOmplete ULTRA Mini EDTA-free protease inhibitor cocktail tablet (Roche, 05892791001), 1 x PhosSTOP phosphatase inhibitor cocktail tablet (Roche, 04906845001), 2 mM sodium orthovana- date (Sigma, S6508). Cells were disrupted by passing 10 times through a 25 g needle followed by centrifugation for 30 s at 800 g. Total proteins from frozen tissues were extracted in ice-cold extraction buffer (as above) using 50 passes in a glass Teflon homogenizer (Fisher Scientific, 11592543). Samples were centrifuged (800g for 3 min at 4°C) to remove debris and concentrations determined using the Bicinchoninic acid assay kit (Sigma, B9643). Twenty to 40 µg protein was mixed with Laemmli buffer at 1:1 v/v ratio with 2.5% v/v β-mercaptoethanol, heated for 5 min at 95°C, then chilled on ice prior to gel loading. Samples were separated on Any-Kd Mini-protean TGX ready gels (Bio-Rad, 456–9034) and electro-blotted onto Hybond-P membranes (GE Healthcare, RPN303F). Blots were blocked in 5% w/v non-fat milk powder in 1x Tris buffered saline (TBST; 50 Mm Tris, 150 mM NaCl, 0.01% v/v Tween-20, Sigma T1503, S7653 and P1379, respectively), for 1 h prior to probing with primary antibody diluted in the same blocking buffer (overnight at 4°C or 2 h at room temperature), then washed (3 times) with 1 x TBST for 10 min and incubated with the appropriate horseradish peroxidase-conjugated secondary antibody; anti-mouse 1:10:000 (Sigma, A4416), anti-rabbit 1:5000 (Sigma, A6154) overnight at 4°C or 1 h at room temperature. Specific protein bands were visualized using Luminata Classico or Forte chemiluminescent substrates (Merck Millipore, WBLUC0500 and WBLUF0500, respectively), images were obtained using a ChemiDoc MP system (Bio-Rad, Hertfordshire, UK). Densitometric analyses were performed using the integrated density measurement function of ImageJ software. All experiments were repeated at least 3 times in triplicate throughout.

Large pore and cell death assays

For dye uptake assays, cells were incubated in the Large Pore (LP) buffer (145mM NaCl, 5mM KCl, 1mM $MgCl_2$ and 10mM Na-HEPES) containing 5µM ethidium bromide (EtBr). Following addition of agonists, EtBr uptake was analysed under LSM510 confocal microscope (Zeiss) with heated stage and a dipping objective, or using POLARstar Optima plate reader (BMG Labtech). Cell death was assessed by LDH release, measured using *in vitro* toxicology assay kit (Sigma) as described in Young et al. (2015).

Intracellular Ca^{2+} measurements

Muscle cells were cultured on glass coverslips in a 6-well plate (500,000 cells/well) for 48 h under conditions described above. Cells (70–80% confluent) were loaded with Fura-2 AM (Molecular Probes, Oregon) in culture medium for 15 min at 37°C in a 95% O_2, 5% CO_2 atmosphere. After two brief washes in the assay buffer (5mM KCl, 1mM $MgCl_2$, 0.5mM Na_2HPO_4, 25mM HEPES, 130mM NaCl, 1mM pyruvate, 5mM D-glucose, and 2mM $CaCl_2$; pH 7.4), the coverslips were

mounted in a cuvette and maintained in the assay buffer at room temperature in RF5301PC spectrofluorimeter (Shimadzu). Fluorescence was recorded at 510nm with excitation at 340/380nm. At the end of each experiment the Fura-2 fluorescence was calibrated by addition of 13µM ionomycin to determine maximal fluorescence. Each experiment was repeated at least five times.

Data analysis and statistics

Results are reported as means +/- standard deviation where n refers to number of independent experiments (Browne et al., 2013; Pippel et al., 2017; Young et al., 2015; Rigato et al., 2012). For statistical analysis, a one-way analysis of variance (ANOVA) was performed with the post- hoc Tukey's test (Microcal Origin 7.0). Differences were considered statistically significant at $p<0.05$.

Acknowledgments: We thank Drs. Paul Cox and Andy Pickford, University of Portsmouth, UK for advice regarding MMP cleavage analysis and Dr F Koch-Nolte, University Medical Centre Hamburg-Eppendorf for the HEK293-P2X7 cells.

Funding: This research was supported by grants from the Muscular Dystrophy Association (MDA) USA to D.C.G. (MDA294571), the National Science Centre, Poland according to the decision number DEC-2013/11/B/NZ3/01573 (to K.Z., J.R., D.C.G.), and EU Interreg grants to D.V. and D.C.G. R.A.-K. was supported by the Higher Committee for Education Development in Iraq (HCED).

Conflict of interest: None.

REFERENCES

1. de Torre-Minguela, C., Barberà-Cremades, M., Gómez, A. I., et al. (2016). Macrophage activation and polarization modify P2X7 receptor secretome influencing the inflammatory process. *Sci. Rep*. 6, 22586.

2. Bartlett, R., Stokes, L., and Sluyter, R. (2014). The P2X7 Receptor Channel: Recent Developments and the Use of P2X7 Antagonists in Models of Disease. *Pharmacol. Rev.* 66, 638-675.

3. Browne, L.E., Compan, V., Bragg, L., et al. (2013). P2X7 Receptor Channels Allow Direct Permeation of Nanometer-Sized Dyes. *J. Neurosci*. 33, 3557-66.

4. Pippel, A., Stolz, M., Woltersdorf, R., et al. (2017). Localization of the gate and selectivity filter of the full-length P2X7 receptor. *Proc. Nat. Acad. Sci.* 114, 2156-2165.

5. Young, C. N. J., Sinadinos, A., Lefebvre, A., et al. (2015). A novel mechanism of autophagic cell death in dystrophic muscle regulated by P2RX7 receptor large-pore formation and HSP90. *Autophagy.* 11, 113-130.

6. Rigato, C., Swinnen, N., Buckinx, R., et al. (2012). Microglia Proliferation Is Controlled by P2X7 Receptors in a Pannexin-1-Independent Manner during Early Embryonic Spinal Cord Invasion. *J. Neurosci.* 32, 11559-11573.

7. Amoroso, F., Falzoni, S., Adinolfi, E., et al. (2012). The P2X7 receptor is a key modulator of aerobic glycolysis. *Cell Death Dis*. 3, e:370.

8. Xia, J., Yu, X., Tang, L., et al. (2015). P2X7 receptor stimulates breast cancer cell invasion and migration via the AKT pathway. *Oncol. Rep*. 34, 103-110.

9. Young, C. N. J., Brutkowski, W., Lien, C. F., et al. (2012). P2X7 purinoceptor alterations in dystrophic *mdx* mouse muscles: Relationship to pathology and potential target for treatment. *J. Cell. Mol. Med.* 16, 1026-1037.

10. Sinadinos, A., Young, C. N. J., Al-Khalidi, R., et al. (2015). P2RX7 Purinoceptor: A Therapeutic Target for Ameliorating the Symptoms of Duchenne Muscular Dystrophy. *PLoS Med.* 12, e:1001888.

11. Gu, B. J., and Wiley, J. S. (2006). Rapid ATP-induced release of matrix metalloproteinase 9 is mediated by the P2X7 receptor. *Blood.* 107, 4946-4953.

12. Visse, R., and Nagase, H. (2003). Matrix metalloproteinases and tissue inhibitors of metalloproteinases: Structure, function, and biochemistry. *Circ. Res.* 92, 827-839.

13. Page-McCaw, A., Ewald, A. J., and Werb, Z. (2007). Matrix metalloproteinases and the regulation of tissue remodelling. *Nat. Rev. Mol. Cell Biol.* 8, 221-33.

14. Yonemura, S., Hirao, M., Doi, Y., et al. (1998). Ezrin/radixin/moesin (ERM) proteins bind to a positively charged amino acid cluster in the juxta-membrane cytoplasmic domain of CD44, CD43, and ICAM-2. *J. Cell Biol.* 140, 885-895.

15. DesMarais, V., Ghosh, M., Eddy, R., et al. (2005). Cofilin takes the lead. *J. Cell Sci.* 118, 19-26.

16. Li, Y., Harada, T., Juang, Y.-T., et al. (2007). Phosphorylated ERM Is Responsible for Increased T Cell Polarization, Adhesion, and Migration in Patients with Systemic Lupus Erythematosus. *J. Immunol.* 178, 1938-1947.

17. Qiu, Y., Li, W. H., Zhang, H. Q., et al. (2014). P2X7 mediates ATP-driven invasiveness in prostate cancer cells. *PLoS One*. 9, e:114371.

18. Vandooren, J., Geurts, N., Martens, E., et al. (2013). Zymography methods for visualizing hydrolytic enzymes. *Nat. Methods*. 10, 211-220.

19. Thompson, O., Kleino, I., Crimaldi, L., et al. (2008). Dystroglycan, Tks5 and Src mediated assembly of podosomes in myoblasts. *PLoS One. 3*, e:3638.

20. Yamada, H., Saito, F., Fukuta-Ohi, H., et al. (2001). Processing of beta-dystroglycan by matrix metalloproteinase disrupts the link between the extracellular matrix and cell membrane via the dystroglycan complex. *Hum. Mol. Genet*. 10, 1563-1569.

21. Sbardella, D., Sciandra, F., Gioia, M., et al. (2015). α-dystroglycan is a potential target of matrix metalloproteinase MMP-2. *Matrix Biol.* 41, 2–7.

22. Michaluk, P., Kolodziej, L., Mioduszewska, B., et al. (2007) β-dystroglycan as a target for MMP-9, in response to enhanced neuronal activity. *JBC.* 282, 16036-16041.

23. Chetty, C., Vanamala, S. K., Gondi, C. S., et al. (2012). MMP-9 induces CD44 cleavage and CD44 mediated cell migration in glioblastoma xenograft cells. *Cell. Signal.* 24, 549-559.

24. Moura, G., Lucena, S., Lima, M., et al. (2015). Post-translational allosteric activation of the P2X7 receptor through glycosaminoglycan chains of CD44 proteoglycans. *Cell Death Discov.* 5, 15005.

25. Thrailkill, K. M., Moreau, C. S., Cockrell, G., et al., (2005). Physiological matrix metalloproteinase concentrations in serum during childhood and adolescence, using Luminex® Multiplex technology. *Clin. Chem. Lab. Med*. 43, 1392-1399.

26. Weitoft, T., Larsson, A., Manivel, V. A., et al. (2015). Cathepsin S and cathepsin L in serum and synovial fluid in rheumatoid arthritis with and without autoantibodies. *Rheumatology (Oxford).* 54, 1923-1928.

27. Artigas, J., Garcia, M., Faure, M., et al. (1981). Serum trypsin levels in acute pancreatic and non-pancreatic abdominal conditions. *Postgrad. Med. J.* 57, 219-22.

28. Ma, B. (2015). The role of P2X7 receptor in estrogen-induced proliferation of breast cancer cells. *FASEB J*. *29*, 845.3.

29. Monif, M., O'Brien, T. J., Drummond, K. J., et al. (2014). P2X7 receptors are a potential novel target for anti-glioma therapies. *J. Inflamm*. 11, 25.

30. Di Virgilio, F., Ferrari, D., and Adinolfi, E. (2009). P2X7: a growth-promoting receptor—implications for cancer. *Purinergic Signal.* 5, 251-256.

31. Rawat, R., Cohen, T. V, Ampong, B., et al. (2010). Inflammasome up-regulation and activation in dysferlin-deficient skeletal muscle. *Am. J. Pathol.* 176, 2891-2900.

32. Gazzerro, E., Baldassari, S., Assereto, S., et al. (2015). Enhancement of muscle T regulatory cells and improvement of muscular dystrophic process in *mdx* mice by blockade of extracellular ATP/P2X axis. *Am. J. Pathol*. 185, 3349-3360.

33. Thompson, O., Moore, C. J., Hussain, S.-A., et al. (2010). Modulation of cell spreading and cell-substrate adhesion dynamics by dystroglycan. *J. Cell Sci.* 123, 118-127.

34. Kwan, J. A., Schulze, C. J., Wang, W., et al. (2004). Matrix metalloproteinase-2 (MMP-2) is present in the nucleus of cardiac myocytes and is capable of cleaving poly (ADP-ribose) polymerase (PARP) *in vitro*. *FASEB J.* 18, 690-692.

35. Schwarz, N., Drouot, L., Nicke, A., et al. (2012). Alternative splicing of the N-terminal cytosolic and transmembrane domains of P2X7 controls gating of the ion channel by ADP-ribosylation. *PLoS One.* 7: e41269.

36. Hadler-Olsen, E., Solli, A. I., Hafstad, A., et al. (2015). Intracellular MMP-2 activity in skeletal muscle is associated with type II fibers. *J. Cell. Physiol*. 230, 160-169.

37. Ali, M. A. M., Chow, A. K., Kandasamy, A. D., et al. (2012). Mechanisms of cytosolic targeting of matrix metalloproteinase-2. *J. Cell. Physiol*. 227, 3397-3404.

38. Adinolfi, E., Raffaghello, L., Giuliani, A. L., et al. (2012). Expression of P2X7 receptor increases *in vivo* tumor growth. *Cancer Res.* 72, 2957-2969.

39. Di Virgilio, F. (2015). Molecular & Cellular Oncology P2RX7: a receptor with a split personality in inflammation and cancer. *Mollecular Cell. Oncol*. 3, e:1010937.

40. Cerami, E., Gao, J., Dogrusoz, U., et al. (2012). The cBio Cancer Genomics Portal: An open platform for exploring multidimensional cancer genomics data. *Cancer Discov.* 2, 401-404.

41. Shiba, N., Miyazaki, D., Yoshizawa, et al. (2015). Differential roles of MMP-9 in early and late stages of dystrophic muscles in a mouse model of Duchenne muscular dystrophy. *Biochim. Biophys. Acta.* 1852, 2170-2182.

42. Hindi, S. M., Shin, J., Ogura, Y., et al. (2013). Matrix Metalloproteinase-9 Inhibition Improves Proliferation and Engraftment of Myogenic Cells in Dystrophic Muscle of *mdx* Mice. *PLoS One*. 8, e:72121.

43. Miyazaki, D., Nakamura, A., Fukushima, K., et al. (2011). Matrix metalloproteinase-2 ablation in dystrophin-deficient *mdx* muscles reduces angiogenesis resulting in impaired growth of regenerated muscle fibers. *Hum. Mol. Genet*. 20, 1787-1799.

44. Cathcart, J., Pulkoski-Gross, A., and Cao, J. (2015). Targeting matrix metalloproteinases in cancer: Bringing new life to old ideas. *Genes Dis*. 2, 34-43.

45. Itoh, T., Matsuada, H., Tanioka, M., et al. (2002). The role of Matrix Metalloproteinase-2 Matrix Metalloproteinase-9 in Antibody-Induced Arthritis. *J Immunol.* 169, 2643-2647.

46. Xue, M., McKelvey, K., Shen, K., et al. (2014). Endogenous MMP-9 and not MMP-2 promotes rheumatoid synovial fibroblast survival, inflammation and cartilage degradation. *Rheumatology (Oxford)*. 53, 2270-2279.

47. Martignetti, J, A., Aqeel, A, A., Sewairi, W, A., et al. (2001). Mutation of the matrix metalloproteinase 2 gene (MMP2) causes a multicentric osteolysis and arthritis syndrome. *Nat. Gen.* 28, 261-265.

48. Cauwe, B., and Opdenakker, G. (2010). Intracellular substrate cleavage: a novel dimension in the biochemistry, biology and pathology of matrix metalloproteinases. Crit. Rev. Biochem. *Mol. Biol.* 45, 351-423.

49. Schindelin, J.; Arganda-Carreras, I., Frise, E. et al., (2012). Fiji: an open-source platform for biological-image analysis. *Nat. Methods.* 9, 676-682.

50. Chan, F. K. M., Moriwaki, K., and De Rosa, M. J. (2013). Detection of necrosis by release of lactate dehydrogenase activity. *Methods Mol. Biol*. 979, 65-70.

FIGURE LEGENDS

Figure 1: MMP-2 activity is constitutively upregulated in dystrophic myoblasts and is released following P2X7 activation. (**A**) IGZ showed MMP-2 activity being significantly upregulated in dystrophic cells, whilst MMP-9 activity being downregulated. (**B**) Western blot showed MMP-2 and 9 protein levels not corresponding with their activity. (**C**) IGZ revealed that in dystrophic but not WT myoblasts ATP (3mM) produced a rapid and significant release of active MMP-2. (**D**) Quantification of MMP-2 activity in IGZ from pellets and supernatants (SuperN) of dystrophic myoblasts. Immunoblot analysis using anti-MMP-2 antibody confirmed the decrease of MMP-2 in *mdx* cell pellets. (**E**) MMP-2 protein was released from dystrophic myoblasts following BzATP (0.5 mM) treatment; this effect was blocked by the P2X7 LP antagonist A438079 (10μM). (**F**) Quantification of MMP-2 protein levels in cell pellets following BzATP treatment +/- A438079. (**G**) MMP-2 protein was concomitantly detectable in concentrated cell culture supernatants from treated cells. (**H**) Time-dependent relationship between MMP-2 protein and LDH levels in *mdx* myoblast supernatants following BzATP treatment.(**I**) P2X7 involvement in MMP-2 release was confirmed in IGZ using pellets and supernatants from myoblasts treated with the selective P2X7 agonist, BzATP +/- 10 min pre-incubation with 10μM P2X7 antagonist A438079. (**J**) Quantification of MMP-2 activity in *mdx* myoblast supernatants following BzATP treatment over 60mins. Where three replicates are shown, these represent three independent biological samples. Actin and total protein (Coomassie staining) band intensities are shown as loading controls. Molecular weight markers in IGZ are shown as a guide only. **P*<0.05, ****P*<0.001.

Figure 2: P2X7-dependent cleavage of cell surface receptors following MMP-2 release. (**A**) In serum-free medium dystrophic myoblasts exposed for 30 min to BzATP displayed cleavage of β-dystroglycan revealing a strong 30 kDa band. (**B**) Quantification of native and cleaved β-dystroglycan protein levels in *mdx* myoblasts following BzATP treatment over 60min (**C**). P2X7-dependent cleavage of CD44 in BzATP-treated *mdx* myoblasts released a ~25 kDa band. (**D**) Quantification of native and cleaved CD44 protein levels following BzATP treatment in *mdx* myoblasts. This P2X7-dependent degradation was absent in WT myoblasts, which lack P2X7 expression (A and C, upper panels). TA = *tibialis anterior*. **P*<0.05, ****P*<0.001.

Figure 3: MMP-2 activity suppresses P2X7 functions. (**A,** upper panel) Exposure of *mdx* myoblasts to ATP in the presence of FBS (with high levels of MMP activity) produced no detectable change in MMP-2 activity in cell pellets irrespective of the ATP concentration used (0.1-1 mM) and did not induce any P2X7-dependent EtBr uptake (**B,** bottom panel). In the absence of serum, MMP-2 activity was released from cells (activity decreased in cell pellets) following stimulation with increasing ATP concentrations (**A**, lower panel). (**B**) Unlike bovine (FBS) and horse (DHS) sera containing high MMP activity, the serum-replacement medium (KSR) is MMP-free and in KSR but not in FBS or DHS, the ethidium bromide (EtBr) fluorescence was observed. (**C**) Quantification of EtBr uptake in *mdx* myoblasts treated with ATP in different sera concentrations. (**D**) Specific MMP-2 inhibitor caused a dose-dependent reduction of MMP-2 activity, which (**E)** correlated with enhanced EtBr uptake and confirmed the role of MMP-2 in this response. EtBr uptake was also reversed by the addition of active recombinant mouse MMP-2 or MMP-2-containing serum (FBS, 5%). (**F**) Calcium influx via P2X7 channels was also inhibited in the presence of recombinant or serum-born MMP-2 activity. (**G**) Diagrammatic representation summarizing the proposed temporal relationship between P2X7 receptor function and MMP-2 activity. Scale bar = 10μm. **P*<0.05, ****P*<0.001.

Figure 4: P2X7-dependent MMP-2 release occurs in macrophages and P2X7-transfected HEK cells. Raw264 mouse macrophages showed a rapid release of MMP-2 following BzATP stimulation (A, top panels) and this response was completely blocked when cells were treated

with BzATP in the presence of 10% FBS (**A**, lower panels). (**B**) Quantification of MMP-2 activity in pellets of BzATP-treated Raw264 cells +/- FBS (10%). (**C**) The same effect was observed in wild type (C57BL10) primary peritoneal macrophages but not in the P2X7 ablated (*mdx*/P2X7$^{-/-}$) macrophages. (**D**) Quantification of MMP-2 activity in pellets and supernatants (SuperN) from peritoneal macrophages following BzATP stimulation. Activation of P2X7 and the MMP release in macrophages were associated with β-dystroglycan cleavage (**E** & **F**) and the P2X7-evoked EtBr uptake (**G**) was augmented by MMP-2 inhibitor but reduced by the exposure to active recombinant MMP2. (**H**) IGZ showing MMP-2 activity in treated cell supernatants from HEK cells transfected with P2X7 demonstrating up-regulated MMP-2 activity and P2X7-dependent MMP-2 release. No detectable MMP-9 activity in these cells confirmed the MMP-2 specific effect. **P*<0.05, ****P*<0.001.

Figure 5: P2X7 is a proteolytic target for MMP-2. (**A,** upper panel) Stimulation with BzATP, shown to trigger active MMP-2 release, was associated with reductions in the 80 kDa P2X7 band in Western blots of dystrophic myoblasts (3 biological replicates shown). (**A,** lower panel) Reduction of the 80 kDa P2X7 band was concomitant with the appearance of an approx. 35 kDa band detected with the antibody targeting the C-terminus of P2X7. This 35 kDa band was absent when samples were treated with BzATP in the presence of the MMP-2 Inhibitor I. (**B**) Quantification of the cleavage product vs. the native protein band estimated it to be approx. 40% and there was no cleaved product if the MMP-2 inhibitor was used. (**C**) Time course experiment showing cleavage to occur 5-15 mins following P2X7 activation. (**D**) Quantification of P2X7 cleavage product level over time. (**E**) The 35 kDa cleavage product was identified in samples from peritoneal macrophages and P2X7-transfected HEK cells (HEK^{P2X7}) and found following sample incubation (30 min, 37^{o}C) with activated recombinant MMP-2 (recMMP-2 active). It was completely absent in samples treated with an inactive enzyme (recMMP-2, pro). (**F**) Quantification of P2X7 native protein and cleaved band levels in cell samples following incubation with recombinant MMP-2. (**G**) Cleavage site prediction (CleavPredict) identified several potential MMP-2 sites in the mouse P2X7 sequence (Uniprot ID, Q9Z1MO) and those corresponding to C-term fragments of approx. 35 kDa are shown. PWM = position weight matrix score. ****P*<0.001.

Figure 6: MMP-2 release prevents LP formation and death despite high P2X7 expression in human prostate cancer cells. (**A**) Western blot of significantly higher P2X7 expression in the LNCaP cancer cell line than in dystrophic myoblasts, shown here as a positive control (*mdx* mbs.) P2X7 expression in LNCaP lysates was not altered following BzATP treatment. (**B**) The LNCaP cells displayed low levels of EtBr uptake following P2X7 stimulation with ATP but EtBr uptake was significantly elevated in the presence of MMP-2 inhibitor. Addition of recMMP-2 ablated this effect as did the presence of 10% serum (DHS). Graph shows the signal as % of the EtBr uptake triggered by digitonin-induced membrane permeabilisation. (**C**) In-gel zymography in LNCaP cell lysates and culture supernatants following 30 min treatment with BzATP showed a significant constitutive release of MMP-2 and 9, elevated further by P2X7 stimulation. (**D**) LDH release assay used as a measure of cell death (Chan et al., 2013). Following 60 min stimulation with 3mM ATP there was very low cell death, which was completely suppressed by the serum (10% DHS) but very significantly enhanced in cells treated with the MMP-2 inhibitor. **P*<0.05, ****P*<0.001.

Figure 7: P2X7 ablation reduces MMP activity in dystrophic muscles *in vivo*. (**A**) *In situ* zymography in cryosections of 8 week old *mdx tibialis anterior* muscle using a fluorophore-quenched gelatin substrate demonstrated a significant upregulation of MMP activity (green) in infiltrating immune cell populations (F4/80 macrophage marker shown in red) and also in and around central nuclei of regenerating myofibers (inset). This activity was significantly reduced in *mdx*/P2X7$^{-/-}$ muscles and in the presence EDTA (right panel). (**B**) Quantification of ISZ activity in TA muscle sections. (**C**) Immunoblotting showing that MMP-2 protein levels were actually reduced in *mdx*

compared to WT muscles whilst there was no significant difference between *mdx* and *mdx*/P2X7$^{-/-}$ samples - a result in clear contrast to the activity levels of these enzymes. **P*<0.05.

Figure 8: Mechanism of P2X7-dependent pore formation, MMP-2 activation and its functional consequences. (Left panel) β-dystroglycan binds α-dystroglycan which interacts with extracellular matrix proteins (e.g.) laminin. CD44 binds ERM proteins, which in turn bind actin, forming a link between membrane and cytoskeleton. P2X7 C-terminus associates with Hsp90, which binds to and stabilizes MMP-2. (Right panel) Following sustained P2X7 stimulation the "large pore" response is activated; MMP-2 is released, facilitating β-dystroglycan degradation disrupting links with both intra and extracellular scaffolds. The extracellular CD44 cleavage product may bind to and augments P2X7 function (Michaluk et al., 2007) while MMP-2 activity halts all P2X7 functions through a direct receptor cleavage.

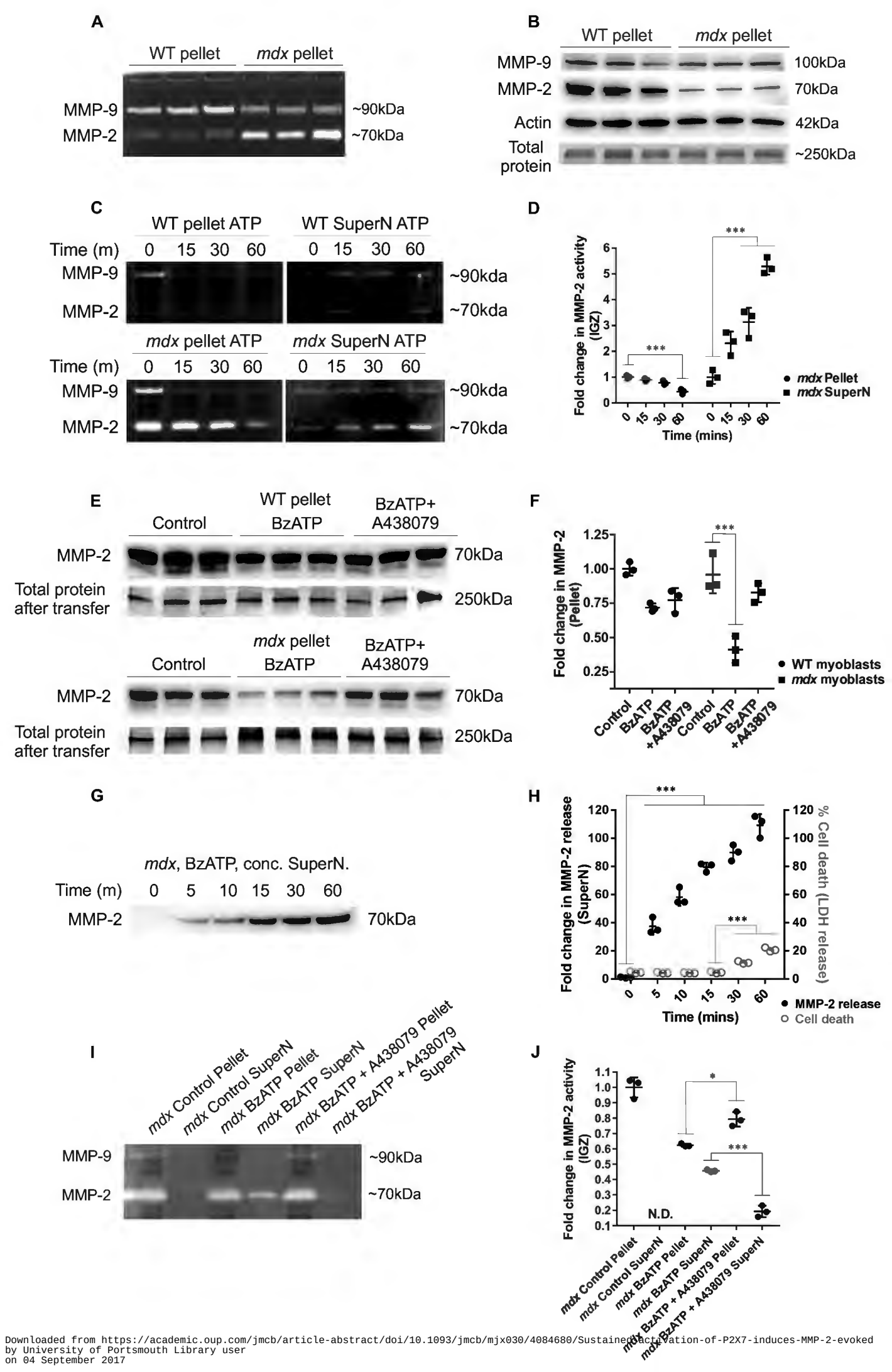

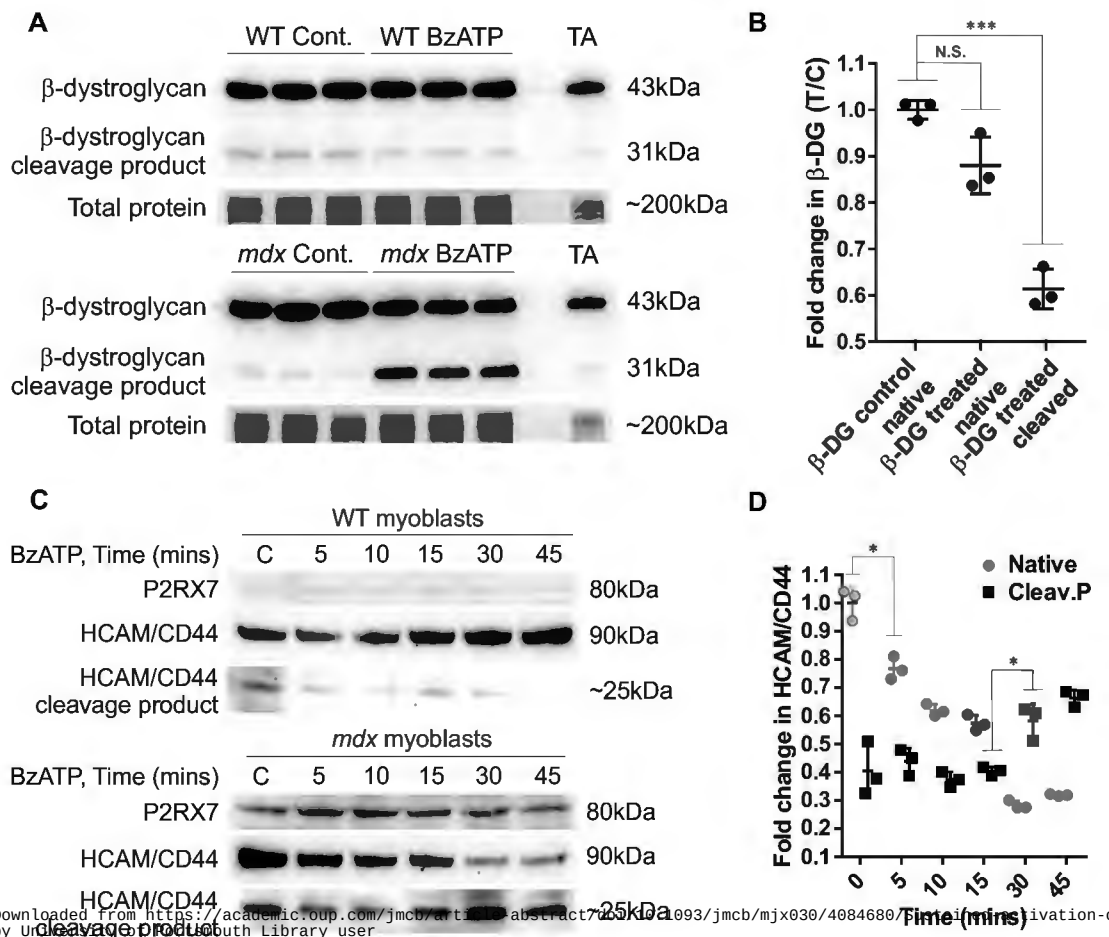

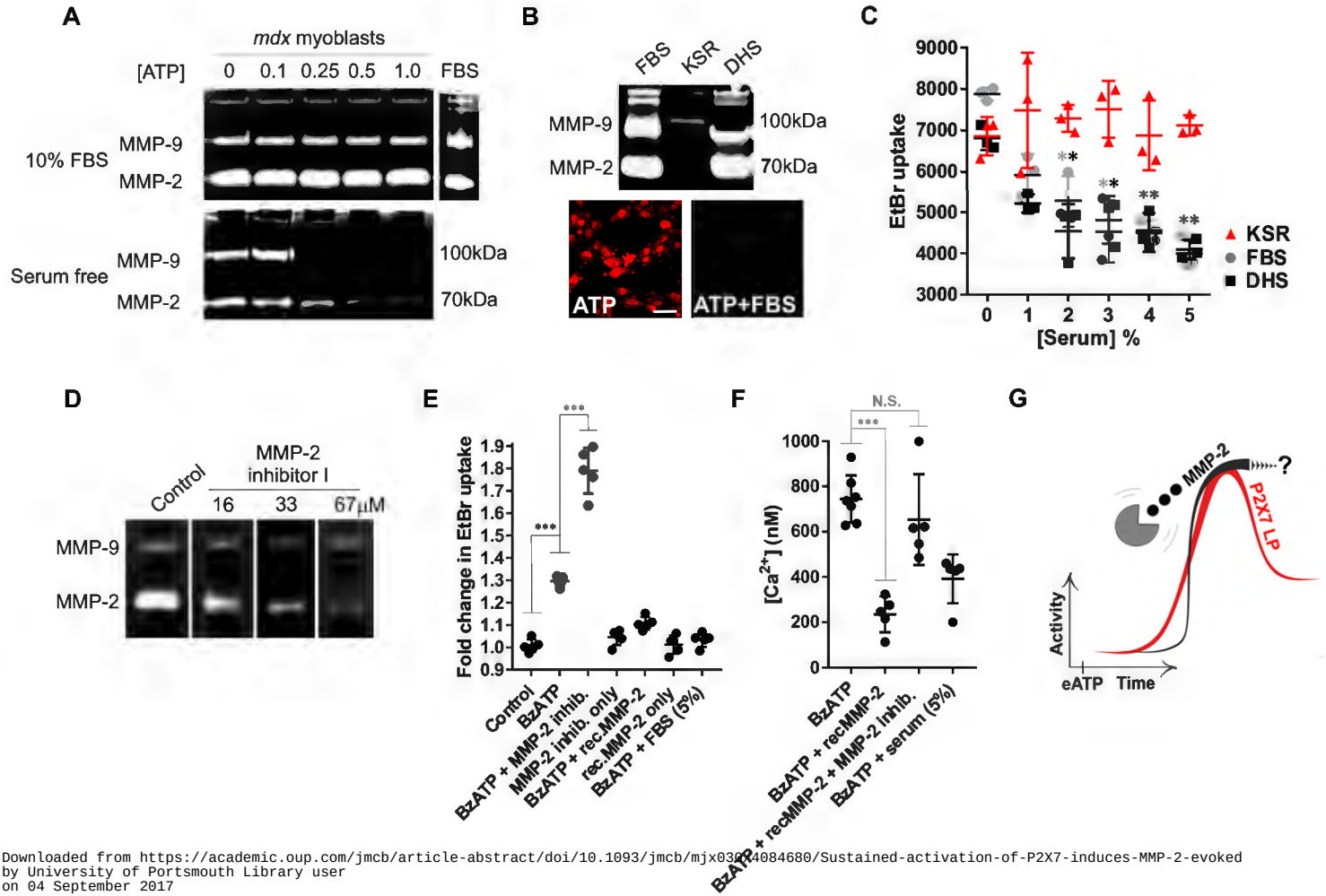

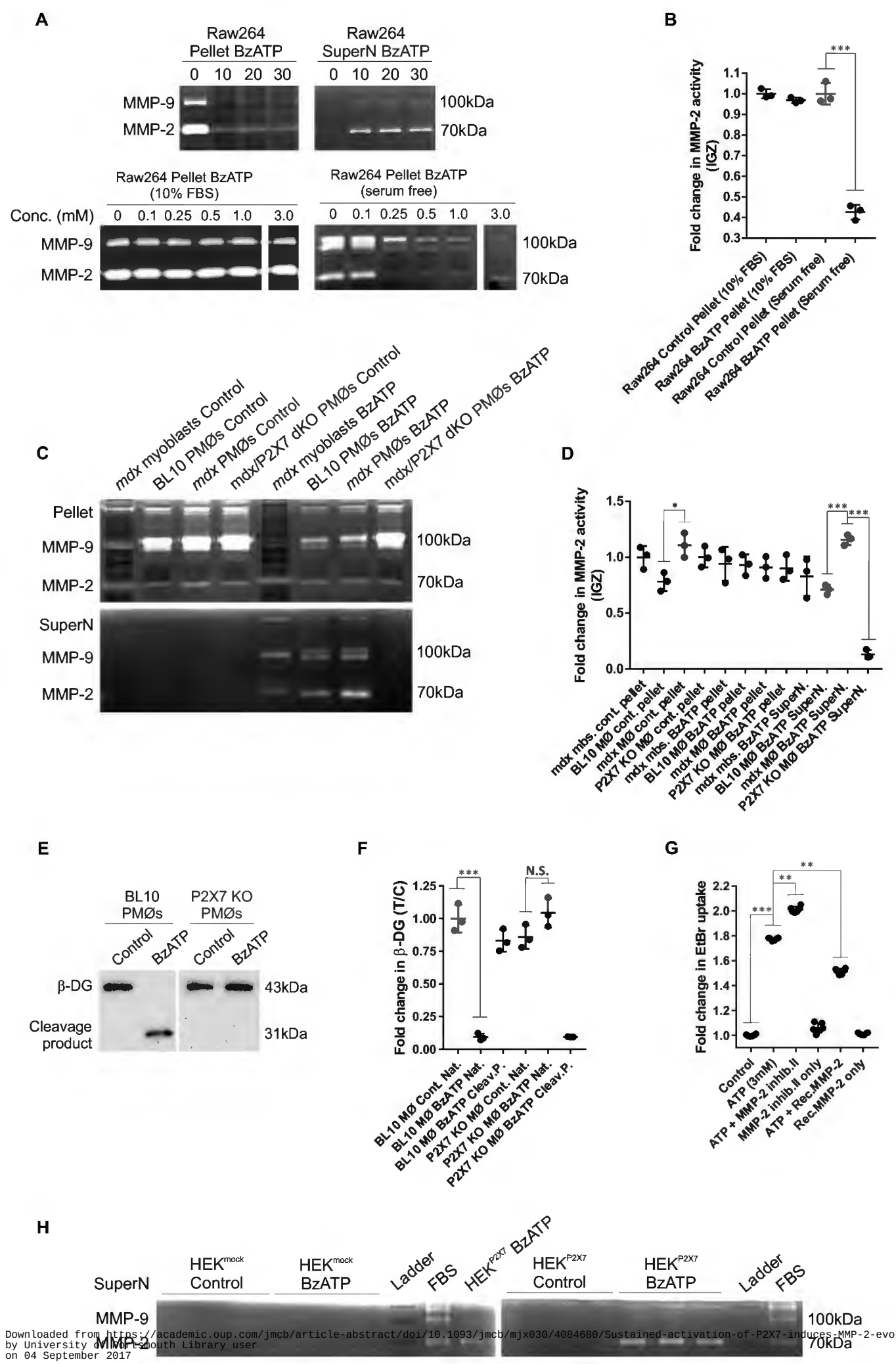

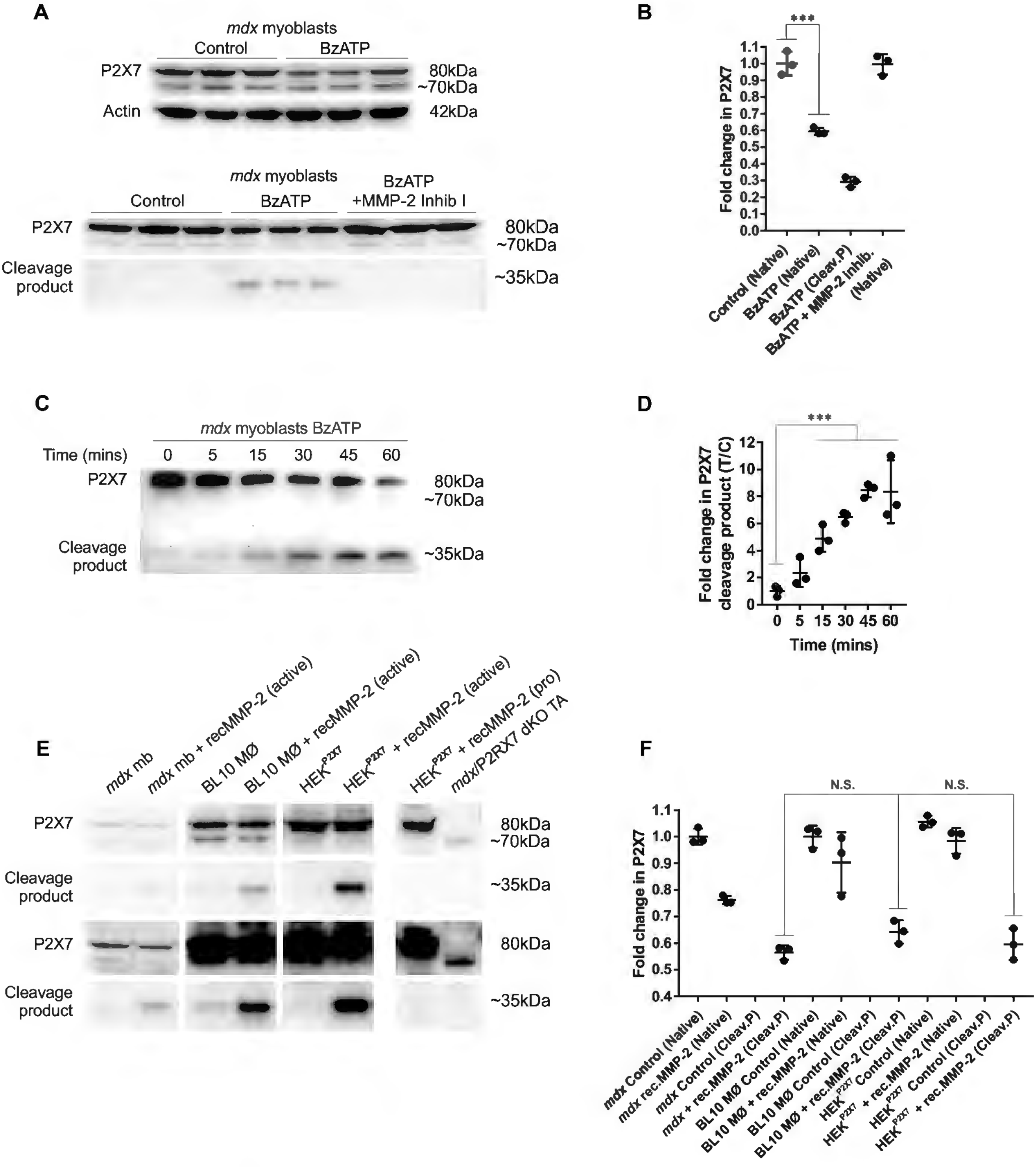

G

P1 ^ pos	Residues	PWM ^ Score	N-mass	C-mass
277	YSFRR-LDDKN	0.83	31663.19	36698.03
[illegible]	[illegible]	[illegible]	[illegible]	[illegible]